Parametric Analysis of the Effect of Concrete Quality on the Seismic Deflection Response of Low, Mid, and High-Rise Reinforced Concrete Buildings Based on SNI 1726:2019

Yoda Karunia Kuntoro[a*]

[a]Department of Civil Engineering, Widya Karya Catholic University, 65115, Indonesia
Corresponding author: yodakarunia1@gmail.com

ARTICLE INFO

Keywords:
Concrete quality
Reinforced concrete
Inter-level deviation
Seismic performance
Parametric analysis
Multi-storey buildings

ABSTRACT

This study aims to parametrically analyse the effect of concrete quality variations on the seismic response of reinforced concrete buildings in the low, medium and high categories, referring to SNI 1726:2019. The high seismic activity in Indonesia demands an in-depth understanding of the behaviour of structures in earthquakes, particularly with respect to deformation. This study quantitatively investigates the impact of five concrete grade variations (fc' 20, 25, 30, 35, and 40 MPa) on the maximum lateral deviation of the roof, the maximum inter-storey deviation ratio (IDR) and its location, and the IDR distribution profile. The research methodology involves response spectrum analysis on 15 three-dimensional building models (3, 6, and 12 storeys) using ETABS software. To maintain consistency, typical plans and dimensions of structural elements were kept constant across model heights, so that the influence of concrete grade could be isolated. The results show that increasing the concrete grade from 20 MPa to 40 MPa consistently increases the stiffness of the structure, which is characterised by a decrease in the fundamental natural vibrating period by about 15.9%. Consequently, there is a reduction in the maximum lateral deviation of the roof between 26.2% and 29.3% and a decrease in the maximum IDR between 18.8% and 21.3%. Building height affects the deformation pattern, with the maximum IDR occurring at the top floor in low-rise buildings, and shifting to the mid-high floors in medium and high-rise buildings. Although an increase in concrete quality is effective in reducing deformations, for the Banyumas (KDS D, SRPMK) seismic configuration and conditions analysed, an increase in fc' up to 40 MPa is often not sufficient to meet the SNI 1726:2019 permissible IDR limit, especially in low- and medium-rise buildings.

1. Introduction

Indonesia is a country with a high level of seismic activity due to its position at the confluence of some of the world's major tectonic plates [1], [2]. This geographical condition places most parts of Indonesia at significant earthquake risk, thus demanding special attention to earthquake resistance aspects in the design and construction of infrastructure, especially buildings. Reinforced concrete buildings are one of the most common types of structures used in Indonesia for various functions, ranging from residences, offices, educational facilities, to commercial centres [3], [4]. Therefore, an in-depth understanding of the seismic behaviour and performance of reinforced concrete structures is crucial to ensure occupant life safety and minimise economic losses due to structural damage during earthquakes.

One of the crucial aspects in evaluating the seismic performance of buildings is their deformation response to earthquake loads. The main deformation parameters of interest are lateral displacement and inter-story drift ratio (IDR). Lateral displacement, especially at the roof level, gives an idea of the global movement of the structure [5], [6], while IDR, which is the relative displacement between two consecutive floors divided by their height, is an important indicator of the extent of damage to structural (beams, columns) and non-structural (infill walls, partitions, facades) elements [7], [8], [9], [10]. Excessive IDR values can lead to structural instability (P-Delta effect), severe damage to non-structural elements that can endanger occupants, and even structural failure.

To ensure safety and adequate performance of buildings during earthquakes, seismic design standards set limits on allowable deformations. In Indonesia, the Indonesian National Standard (SNI) 1726:2019 on Earthquake Resistance Planning Procedures for Building and Non-Building Structures is the main reference. This standard sets the maximum permissible IDR limit, which is: 1.5% of level height for risk category IV buildings with Special Moment Frames (SMF) for different levels of expected seismic performance, i.e. Life Safety (LS) [11], [12], [13]. Fulfilment of this deformation limit is one of the main targets in the design process of earthquake-resistant structures.

The deformation response of reinforced concrete structures is strongly influenced by the stiffness of the structural elements. The flexural rigidity and shear rigidity of beams, columns and slabs are directly determined by the cross-sectional dimensions of the elements and the properties of their constituent materials, namely concrete and reinforcing steel. In the context of concrete materials, the two main interrelated properties that significantly affect rigidity are the compressive strength of concrete (fc') and its modulus of elasticity (Ec) [14], [15].

SNI 2847:2019 on Structural Concrete Requirements for Building and Explanation provides an empirical relationship between fc' and Ec for normal weight concrete. Based on Article 19.2.2.1.b, the modulus of elasticity of normal concrete can be calculated using the equation:

$Ec = (4700)*(\sqrt{fc})$ (in MPa) [16]

This equation shows that the modulus of elasticity of concrete (Ec), which is a measure of the stiffness of concrete material, is directly proportional to the square root of its compressive strength (fc') [16], [17]. Theoretically, an increase in concrete grade (fc') will result in higher Ec values [18], [19]. This increase in Ec will, in turn, increase the stiffness of structural elements such as flexural stiffness EI, where E is Ec and I is the moment of inertia of the cross section [20], [21], [22]. By increasing the stiffness of the elements and the structure as a whole, it is expected that the deformation

response (deviation and IDR) due to lateral loads such as earthquakes will be reduced.

A number of studies have examined the effect of using high-strength concrete (HSC) or concrete grade variations on structural performance. Some studies show that the use of concrete with higher fc' tends to increase the overall stiffness of the structure, which implies a decrease in the natural vibration period and a reduction in lateral deviation and IDR [23], [24], [25]. For example, studies on low-rise buildings have found that the use of graded concrete (a combination of different grades of concrete in one element) with higher grades in beam components can increase the level stiffness and reduce the vibration period and deviation [24].

Parametric studies are also often conducted to evaluate the sensitivity of seismic response to various design parameters. Commonly varied parameters include element dimensions, reinforcement ratio, shear wall configuration, structural system type (e.g., frame vs. shear wall vs. double system), and material properties [26], [27], [28], [29]. In addition, the influence of building height on seismic response is also an important focus. Buildings of different heights (low, mid, high) exhibit different dynamic behaviour. Low buildings tend to have a response dominated by the first vibrating mode and shear behaviour [30], [31], while tall buildings are more influenced by higher vibrating modes and global bending behaviour [32], [33]. This difference can affect the IDR distribution pattern along the building height, including the location of the maximum IDR [7], [34], [35], [36], [37].

Although many studies have explored the effect of various parameters on seismic performance, there are some aspects that require further investigation. Many studies that vary the concrete grade (fc') often do so in conjunction with changes in other parameters, such as dimensional adjustment of structural elements for design optimisation purposes or due to different standard requirements for different concrete grades. As a result, it becomes difficult to isolate and purely quantify the intrinsic influence of concrete material properties (fc' and Ec) on the deformation response of structures. In addition, studies that systematically and controllably compare the effect of fc' variations at different building height categories (low, mid, and high) while holding the plan geometry and dimensions of the structural elements constant are relatively limited.

This research is designed to fill this gap by adopting a strictly controlled parametric study approach. The main concept is to use one reference building design and adapt it into three building models of different heights (3, 6, and 12 storeys) while keeping the typical plan and cross-sectional dimensions of all structural elements (columns, beams, slabs) identical across all models. In each of these height categories, five concrete grade variations (fc' = 20, 25, 30, 35, and 40 MPa) were applied. This approach effectively isolates the concrete grade variable (fc' and consequently Ec) as the only parameter that changes within each height category.

The scientific value of this approach lies in its ability to directly and quantitatively map the sensitivity of the seismic deformation response (maximum lateral deviation, maximum IDR, and IDR distribution profile) to variations in the base material parameters (fc' and Ec). This is done under controlled structural geometric conditions, at different levels of dynamic complexity represented by three building height categories. The results are expected to provide a clearer understanding of the extent to which concrete grade influences deformation behaviour and how this influence interacts with the dynamic characteristics associated with building height. The main objectives of this research are as follows:

1. Investigate and quantitatively compare the effect of varying concrete grades (fc' = 20, 25, 30, 35, and 40 MPa) on the deformation behaviour of the building:
   - Maximum lateral deviation at roof level.
   - Maximum inter-storey deviation ratio (IDR) (value and location of occurrence).
   - IDR distribution profile along the building height. This was done on three representative reinforced concrete building models: low (3 storeys), mid (6 storeys), and high (12 storeys).
2. Analyse how the interaction between variations in concrete grade and differences in building height affect the seismic deformation response characteristics.
3. Evaluate compliance with the inter-level clearance deviation limits set by SNI 1726:2019 for the various analysed model scenarios..

To achieve this goal, three-dimensional structural analyses were conducted on a total of 15 building models using ETABS structural analysis software. The analysis method used was Response Spectrum Analysis in accordance with the procedures stipulated in SNI 1726:2019. The earthquake parameters used were specific to the location of Banyumas, Central Java. In the modelling, the material properties of concrete and reinforcing steel were defined according to standards, and the effect of cracking on the stiffness of structural elements (columns, beams, slabs) was taken into account using the moment of inertia reduction factor according to SNI 2847:2019.

2. Method

The building used as a reference in this research is the building structure of the Al-Nizam Modern Islamic Boarding School. The building is a 6-storey reinforced concrete structure located in Kebanggan Village, Sumbang District, Banyumas Regency, Central Java Province. The original architectural and structural design data, including typical plan drawings of each floor, cross sections, and longitudinal sections of the building, were used as the basis for geometry modelling.

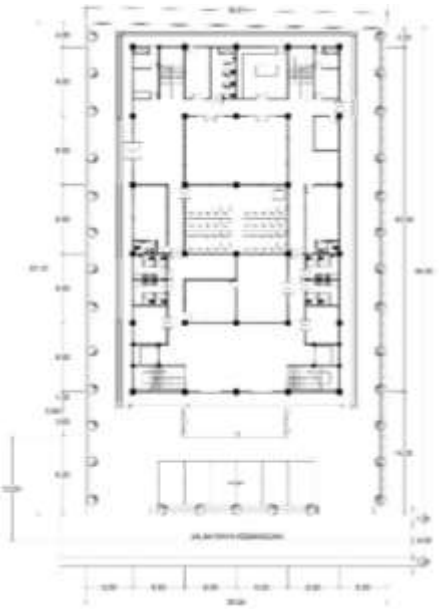

Figure 1 Typical Building Floor Plan

Figure 1 presents a typical floor plan of the Al-Nizam Modern Islamic Boarding School building. This plan represents the layout of spaces and major horizontal structural elements on one representative floor. It can be seen that the overall dimensions of the building are 35.00 metres by 56.80 metres. The long side of the building (56.80 metres) runs from the bottom-left to the top-right of the drawing, while the wide side (35.00 metres) runs from the top-left to the bottom-right. There is an access road at the bottom of the plan. The layout of the structural columns is clearly visible as regularly distributed black-coloured squares. The spacing between columns varies, with main spans of 8.00 metres and 6.00 metres. The plan also identifies general spatial functions, such as open areas, corridors, and the possibility of rooms or classrooms indicated by the division of smaller spaces. The position of stairs and voids can also be identified. This plan forms an important basis for modelling the mass distribution and horizontal stiffness of the structure.

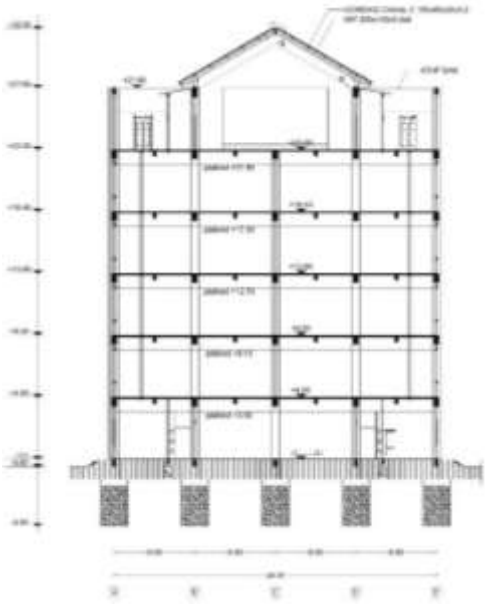

Figure 2 Cross Section

Figure 2 shows a cross-section of the reference building. It provides a two-dimensional view of the building structure when cut vertically across the width of the building. It is clear that the building consists of six storeys above ground level and a single storey roof deck. The elevation of each floor is shown, ranging from an elevation of ±0.00 at ground level to +27.60 at the top level of the roof deck. Typical inter-storey height is 4.60 metres for all floors.

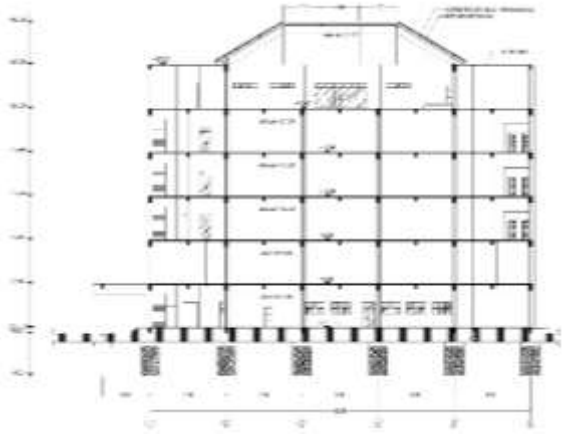

Figure 3 Longitudinal Section

Figure 3 presents a longitudinal section of the reference building. Similar to the cross section, this longitudinal section provides a vertical view of the structure, but taken along the long axis of the building. This drawing again confirms the number of storeys, which is six main storeys and one roof storey. The elevation of each floor is consistent with that shown in Figure 2. Details of the roof structural system with steel trusses and roof deck are also visible. In addition, this section provides an overview of the configuration of openings in the longitudinal facade of the building, such as windows and doors, which are important for understanding the wall load distribution and the interaction between structural and non-structural elements. The sole foundation system is also visible at the bottom of the structure. The combination of information from the typical plan (Figure 1), cross section (Figure 2) and long section (Figure 3) provides a comprehensive understanding of the three-dimensional geometry of the reference building on which the modelling in this study is based.

2.1 Analytical Model Development

To study the effect of the combination of building height and concrete grade, a series of analysis models were developed by varying these two parameters while keeping other geometric aspects constant.

2.1.1 Building Height Variations

Three categories of building heights were modelled based on an adaptation of a 6-storey reference building, maintaining the same typical plan, namely:

- Low-Rise (LR): 3-Storey Building
  This model was created by taking the 1st to 3rd floors of the reference building. All structural elements above the 3rd floor are removed. The total height of this model is H_{LR}.
- Mid-Rise (MR) 6-Storey Building
  This model uses the entire design of the reference building, from floors 1 to 6. The total height of this model is H_{MR}, the same as the height of the original building.
- High-Rise (HR): 12-Storey Building
  This model is created by duplicating each floor of the reference building. The 1st floor of the reference becomes the 1st and 2nd floors of the HR model, the 2nd floor of the reference becomes the 3rd and 4th floors of the HR, and so on until the 6th floor of the reference becomes the 11th and 12th floors of the HR model. The total height of this model

is H_{HR}, which is approximately double that of H_{MR}.

This adaptation approach, particularly for the HR model, ensures that the plan configuration and layout of the vertical elements (columns) remain consistent relative to the number of storeys, allowing valid comparisons of the effect of increased height.

Figure 4 describes the adaptation scheme of a low-rise (LR) building model consisting of 3 floors. This figure is a three-dimensional visualisation of the LR structural model generated using the analysis software. It can be seen that the model retains the typical plan configuration of the reference building, but consists of only three storeys. Structural elements such as columns (coloured cyan and magenta), beams (coloured green and yellow), and floor slabs (coloured transparent magenta and transparent yellow) are clearly represented. The pinch stance at the base of the column is marked with a red coloured symbol. Global coordinate axes (X, Y, Z) are also shown for model orientation. This drawing visually confirms that the LR model is the lower part of the reference structure, with all elements above the third floor removed.

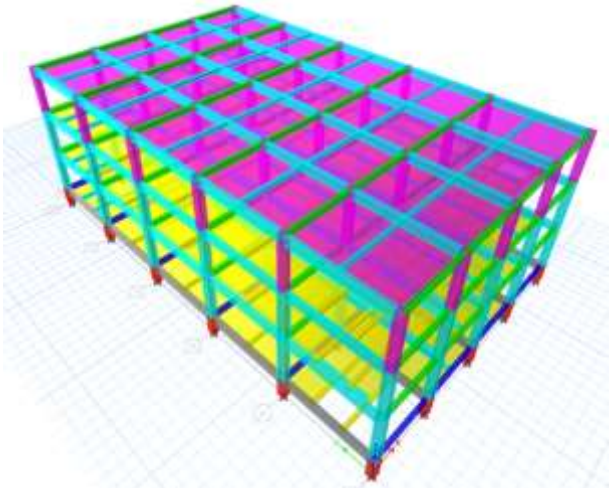

Figure 4 Adaptation Scheme of LR Model (3 storeys) of Reference Building

Figure 5 presents a schematic adaptation of a 6-storey mid-rise (MR) building model. This three-dimensional visualisation shows the MR structural model which is identical to the reference building of Al-Nizam Modern Islamic Boarding School. The model has six storeys with the same typical floor plan on each floor. The representation of structural elements (columns, beams, slabs) and basic framing uses a colour scheme and symbols consistent with Figure 4. This figure serves as a visual representation of the base model prior to further height modification (for HR) or height reduction (for LR).

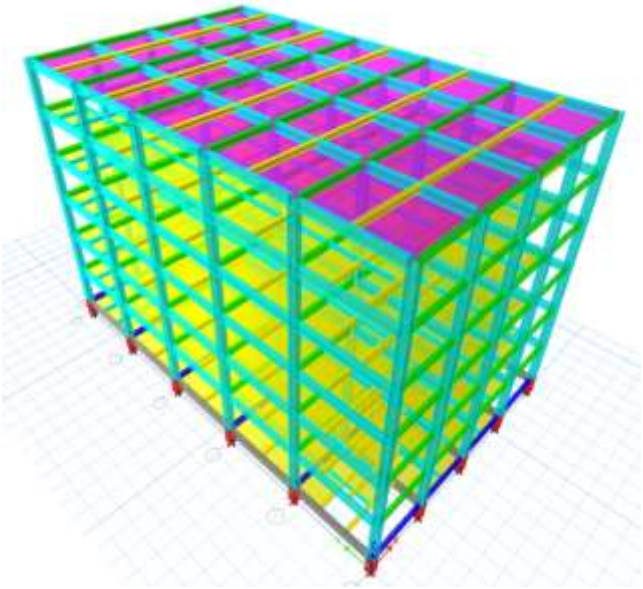

Figure 5 Adaptation Scheme of MR Model (6 storeys) of Reference Building

Figure 6 displays the adaptation scheme of a 12-storey high-rise (HR) building model. The HR model is visualised in three dimensions, showing a significant increase in height compared to the MR model. The adaptation was done by doubling each floor level of the reference building, resulting in a total of 12 floors while maintaining the same typical plan configuration. The colour and representation of the structural elements (columns, beams, slabs) as well as the basic alignment follow the conventions used in Figures 4 and 5. This visualisation helps in understanding the scale of the HR model and how the geometric relationships between floors are maintained despite the increase in the number of floors.

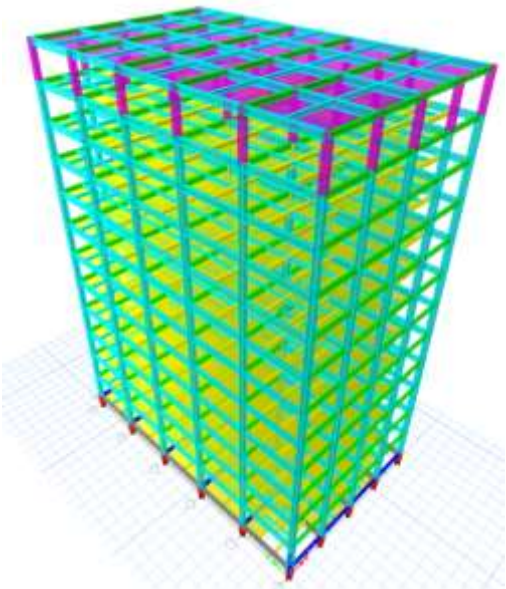

Figure 6 Adaptation Scheme of HR Model (12 storeys) of Reference Building n

2.1.2 Variation of Concrete Quality

For each height category (LR, MR, and HR), five concrete quality variations (28-day-old concrete characteristic compressive strength, fc') were applied to all concrete elements (columns, beams, slabs). The fc' values used were:

- 20 MPa

- 25 MPa
- 30 MPa
- 35 MPa
- 40 MPa

This range includes concrete quality values that are commonly applied in reinforced concrete building construction projects in Indonesia.

2.1.3 Analysis Model Matrix

The combination of the three height categories and five concrete grade variations resulted in a total of 15 unique analysis models. This matrix of analysis models, which summarises the scope of the parametric study conducted, is presented in Table 1. This table visually shows the design of the numerical experiments, facilitating an understanding of the combination of independent variables investigated.

Table 1 Analysis Model Matrix

Model ID	Altitude Category	Number of storey	Concrete Quality (fc') (MPa)
LR-20	Low-Rise (LR)	3	20
LR-25	Low-Rise (LR)	3	25
LR-30	Low-Rise (LR)	3	30
LR-35	Low-Rise (LR)	3	35
LR-40	Low-Rise (LR)	3	40
MR-20	Mid-Rise (MR)	6	20
MR-25	Mid-Rise (MR)	6	25
MR-30	Mid-Rise (MR)	6	30
MR-35	Mid-Rise (MR)	6	35
MR-40	Mid-Rise (MR)	6	40
HR-20	High-Rise (HR)	12	20
HR-25	High-Rise (HR)	12	25
HR-30	High-Rise (HR)	12	30
HR-35	High-Rise (HR)	12	35
HR-40	High-Rise (HR)	12	40

The presentation of the model matrix in Table 1 confirms the systematic approach of this study. By explicitly mapping the 15 unique cases analysed, the table highlights how the independent variables (height and fc') were combined to evaluate their influence on the dependent variable (natural vibration characteristics).

2.2 Structure Geometry

Structural geometry is one of the fundamental factors that affect the natural vibration characteristics of a building. In this study, three different building height categories are analysed: High-Rise (HR) buildings with 12 storeys, Mid-Rise (MR) buildings with 6 storeys, and Low-Rise (LR) buildings with 3 storeys. These three categories are adapted from one reference building design (Pondok Pesantren Modern Al-Nizam), maintaining the same typical plan to ensure consistency of horizontal configuration.

In contrast to the approach of keeping element dimensions constant, this revised methodology adopts different structural element dimensions (columns, beams, slabs) for each height category (HR, MR, and LR). This dimensional adjustment was made to represent a more realistic structural engineering design practice, where element dimensions are optimised based on the building height level and the acting loads. Although the dimensions vary between height categories, it is important to note that within the same height category (e.g., all HR models), the dimensions of the structural elements are kept constant across all variations of concrete grade (fc') to isolate the influence of that material parameter. Details of the specific structural element dimensions for the tall building category (HR) are presented in Table 2 below.

Table 2 Dimensions of Structural Elements of High Category Buildings (HR - 12 Storeys)

No	Structure Elements	Dimensions (mm)
1	1st floor pedestal column	P 600x600
2	2nd - 3rd floor columns	K 600x600
3	4th - 9th floor columns	K 600x600
4	10th - 12th floor columns	K 550x550
5	8 metre span main beam	B 700x350
6	6 metre span main beam	B x500x250
7	Secondary beams	BA 450x250
8	Floor Plates	120 mm
9	Roof Plates	100 mm

Furthermore, for the mid building category (MR), the dimensions of the structural elements used are different from those of the HR and LR categories. This adjustment reflects the structural requirements for buildings with a height of 6 storeys. Details of the structural element dimensions for MR buildings are presented in Table 3.

Table 3 Dimensions of Structural Elements of Mid Category Buildings (MR - 6 Storeys)

No.	Elemen Struktur	Dimensi (mm)
1	1st floor pedestal column	P 600x600
2	2nd - 3rd floor columns	K 600x600
3	2st – 3th floor columns	K 550x550
4	8 metre span main beam	B 700x350

No.	Elemen Struktur	Dimensi (mm)
5	6 metre span main beam	B x500x250
6	Secondary beams	BA 450x250
7	Floor Plates	120 mm
8	Roof Plates	100 mm

Finally, the low-rise (LR) building category consisting of 3 storeys has its own set of structural element dimensions, customised for this height level. These dimensions differ from those used in the MR and HR models. Details of the structural element dimensions for LR buildings can be seen in Table 4.

Table 4 Dimensi Elemen Struktur Bangunan Kategori Rendah (LR - 3 Lantai)

No	Elemen Struktur	Dimensi (mm)
A	1st floor pedestal column	P 600x600
B	2nd - 3rd floor columns	K 600x600
C	8 metre span main beam	B 700x350
D	6 metre span main beam	B x500x250
E	Secondary beams	BA 450x250
F	Floor Plates	120 mm
G	Roof Plates	100 mm

With specific element dimensions defined for each height category (HR, MR, LR) as detailed in Tables 2, 3, and 4, subsequent analyses can evaluate the effect of variations in concrete grade (fc') in the context of representative structural geometries for each building height level.

2.3 Structural Modelling and Analysis

2.3.1 Analysis Software

The software used in this research is ETABS version 22.5.1. ETABS was chosen due to its extensive capabilities in modelling and analysis of building structures, including specific features for seismic analysis according to SNI standards, modelling of frame and shell elements, and handling of non-linear material properties.

2.3.2 Structural Element Modelling

The main structural elements were modelled as follows:

- Columns and beams were modelled using Frame elements (one-dimensional line elements). The section properties (dimensions) were taken from Table 1, while the material properties (fc', Ec, fy, Es) were taken from Table 2 and Table 3 according to the model variation analysed.
- Cracked section properties

  To obtain a more realistic estimate of the stiffness of the structure when it is subjected to earthquake loads (which are assumed to cause cracking in the concrete elements), a moment of inertia reduction factor is applied as per SNI 2847:2019 Article 6.6.3.1.1 Table 6.6.3.1.1(a) [38]. This reduction factor multiplies the gross moment of inertia (Ig) to obtain the effective moment of inertia (Ieff) used in the analysis. The use of the cracking property is important because ignoring it will result in a structure that is too stiff, a vibration period that is too short, and a deviation that is too small compared to the actual behaviour. The reduction factors used are:
  - Columns: Ieff = 0.70 Ig
  - Beams: Ieff = 0.35 Ig
- The floor slab and roof slab were modelled using Shell elements (two-dimensional area elements) with the Shell-Thin formulation. The Shell-Thin formulation ignores transverse shear deformation and is suitable for modelling floor and roof slabs where the ratio of span to thickness is relatively large. The slab thickness is taken from Table 1, and the concrete material properties (fc', Ec) are taken from Table 2.
- The moment of inertia reduction factor for slabs due to cracking is also applied as per SNI 2847:2019 Article 6.6.3.1.1, i.e. Ieff = 0.25 Ig.

2.3.3 Meshing of Plate Elements

To ensure accurate load transfer from the plate element (Shell) to the beam and column elements (Frame) at their intersections, as well as to obtain better stress and strain distribution within the plate itself, the Shell element is divided into smaller elements (meshing). The meshing process is done automatically by ETABS by specifying the maximum mesh size. In this study, the maximum mesh size used is 0.10 metres x 0.10 metres. This fairly small mesh size is expected to provide adequate accuracy without causing excessive computation time.

2.3.4 Floor Diaphragm Modelling

Each floor was modelled assuming a diaphragm to distribute the horizontal lateral loads (due to earthquakes) to the lateral force resisting vertical elements (columns). In this study, the diaphragm assumption used is a semi-rigid diaphragm.

The semi-rigid diaphragm assumption takes into account the actual in-plane stiffness of the floor slab elements modelled as Shell elements. Unlike the rigid diaphragm which assumes infinite stiffness and ignores in-plane deformation, the semi-rigid diaphragm allows for membrane deformation of the slab [39], [40]. Although for buildings with regular plans and solid concrete slabs their effect on global deviation is less than that of rigid diaphragms, the use of semi-rigid assumptions is considered to provide a theoretically more accurate representation of floor behaviour and allow for a more realistic distribution of lateral loads to vertical elements based on the actual relative stiffness of the slab and vertical elements [39], [41].

2.3.5 Boundary Conditions

The structural framing at the ground level (1st floor) is modelled as Fixed Support. This boundary condition assumes that the building foundation is very rigid and the underlying soil is capable of resisting all translational movements (displacements in the X, Y, and Z directions) and all rotations (rotations about the X, Y, and Z axes) at the column support points at the base of the structure [42], [43]. This assumption

is a common simplification in superstructure analysis, where Soil-Structure Interaction (SSI) is neglected. Although SSI can affect the vibration period and deviation response of the structure (generally lengthening the period and possibly increasing the deviation), the use of consistent pinch boundary conditions across all 15 analysis models allows for a valid comparison of the relative effects of varying concrete grades and heights within the scope of this study.

2.4 Loading

Determination of the loads acting on a structure is a crucial stage in building analysis and design. These loads are classified by their nature and source, and must be accounted for in accordance with applicable planning standards to ensure the safety and serviceability of the structure. In this study, the loads reviewed include dead load (DL), supplementary dead load (SDL), live load (LL), earthquake load (EQ), and wind load (WL), which are defined and quantified based on [11], [12], [13], [38], [44].

2.4.1 Dead Load (DL)

Dead load (DL) is the vertical load permanently acting on the structure, derived from the self-weight of the main structural elements that make up the building. This load includes the weight of columns, beams (main and subsidiary), floor slabs, and roof slabs. Dead load calculations are performed automatically by the ETABS software based on the volume of the modelled structural elements (as per the dimensions in Tables 2, 3, and 4) and the specific gravity of the constituent materials. The specific gravity of the main structural materials used in this analysis is summarised in Table 4 below.

Table 5 Specific Gravity of Main Structure Material

No	Material	Specific Gravity(γ) (kN/m³)
1	Reinforced Concrete	24
2	Reinforcing Steel	78,5

2.4.2 Superimposed Dead Load (SDL)

Supplementary dead load (SDL) includes the weight of all building components other than the main structural elements, which are permanent and fixed during the service life of the building. This load includes non-structural elements such as infill walls, floor finishes, ceilings, mechanical, electrical and plumbing (MEP) installations, and other architectural components. In structural analysis, SDL is generally differentiated based on the way it acts on the structural elements, namely as a uniform load on the slab (in kN/m²) or as a line load on the beam (in kN/m).

The SDL load acting as a uniform load on the floor slab and roof slab elements includes the weight of the floor finishing layer (e.g. ceramic and mortar), hanging and ceiling materials, as well as the load allocation for MEP installation. Details of the components and magnitude of the evenly distributed SDL loads assumed for this boarding school building are presented in Table 5.

Table 6 Details of SDL Evenly distributed on the Slab

No	SDL Components on Plates	Load Type (kN/m3)	Load (kN/m²)
1	Sand (5 cm)	17.65197	0,88
2	Cement (2 cm)	0.20593965	0,004
3	Keramik (1 cm)	0.2353596	0.24
4	Ceiling	0.1765197	0.18
5	Mechanical and electrical	0.196133	0.20
Total			1,49

In addition to the uniform load on the slab, there are also SDL loads acting linearly (line) on the beam element, mainly from the weight of the infill wall (e.g. light masonry or red brick) that the beam is supporting. This load is calculated based on the specific gravity of the wall material, thickness, and height of the wall, and then expressed in kN/m of beam length. Details of the calculation of the line SDL load due to the assumed wall are shown in Table 6.

Table 7 SDL Details of Lines on Beams (Due to Walls)

Wall Component	Specific gravity (γ) (kN/m³)	Thickness (t) (m)	Load per Unit Area (kN/m²)
White Brick (AAC) 10 cm	6.0	0.100	0.600
Plastering (2 sides @ 15 mm)	20.4	0.030	0.612
Acian (2 sides @ 3 mm)	20.4	0.006	0.1224
		Total	**1.3344**
Total Wall Load per Unit Area (Wtotal area)			**1.3344**
		Total Linear Load on Beams SDL = Wtotal area × 4.5 m (kN/m)	**6.14**

2.4.3 Live Load (LL)

Live load (LL) is the load acting on the structure due to occupancy or use of the building, which is not permanent and can move or change in magnitude during the service life of the building. The amount of live load is determined based on the function of the space in accordance with the applicable loading standard, namely SNI 1727: 2020. For boarding school buildings that have various space functions, the minimum live load values that must be taken into account are summarised in Table 7, referring to Table 4.3-1 of SNI 1727:2020.

Table 8 Live Load (LL)

No	Space Function	Beban Hidup (kN/m²)
1	Panel room	4,79
2	Toilet	2,87
3	Kitchen	7,18
4	Light warehouse	6,00
5	Computer room	4,79
6	Office Room	2,4
7	First floor corridor	3,83
8	Next floor corridor	4,79
9	Flat roof	0,92
10	Classroom	1,92
11	Bedroom	1,92
12	Hall	2,87
13	Library	2,87

These live loads are applied to the floor slabs according to the functional plan of the building and will be partially accounted for in determining the seismic mass of the structure.

2.4.4 Earthquake Load (EQ)

Earthquake load (EQ) is the dynamic lateral load acting on the structure due to ground motion during an earthquake [46]. The determination of the magnitude of the design earthquake load for structural analysis is carried out based on the procedures set out in SNI 1726:2019 [45], [46]. This process involves several key steps that depend on the geographical location of the building, local soil conditions, the risk level of the building and the structural system used.

First, the spectral response parameters of earthquake acceleration in soft soil (Site Class SE) for the short period (Ss) and 1-second period (S1) based on the geographical location of the building in Banyumas Regency, Central Java were determined using the national earthquake map provided by RSA Puskim application. Furthermore, a classification of the soil type at the building site (Site Class) was conducted based on the soil investigation data. Based on the Site Class and the values of Ss and S1, the site amplification coefficients Fa and Fv were determined from Tables 6 and 7 of SNI 1726:2019.

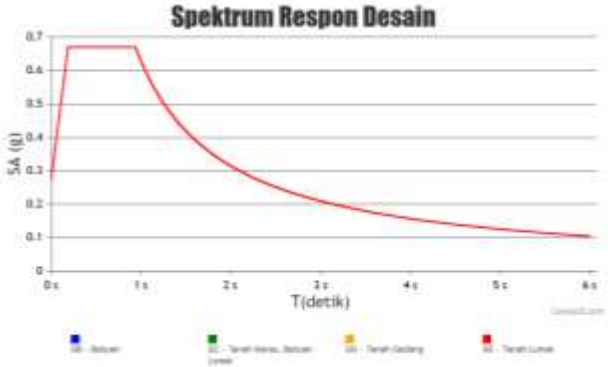

Figure 7 Design Response Spectrum Graph

With the values of Fa, Fv, Ss, and S1, the design earthquake acceleration spectral response parameters at ground level for the short period (SDS) and 1-second period (SD1) are calculated using the formula:

SDS = (2/3) * Fa * Ss

SD1 = (2/3) * Fv * S1.

The building risk category for the Islamic Boarding School is Risk Category IV as an educational facility. The Earthquake Vulnerability Factor (Ie) determined based on the Risk Category (Ie) is 1.50 for Category IV. Based on the Risk Category as well as the SDS and SD1 values, the Seismic Design Category (KDS) of the building (A, B, C, D, E, or F) is determined using Tables 8 and 9 of SNI 1726:2019.

The earthquake force resisting structural system used is the Reinforced Concrete Special Moment Resisting Frame System (SRPMK), which finally determines the structural response parameters, namely the Response Modification Factor (R), System Overpower Factor (Ωo), and Deflection Magnification Factor (Cd), whose values are taken from Table 12 of SNI 1726:2019. Finally, the effective seismic mass of the building is calculated as the sum of all dead loads (DL + SDL) plus a certain percentage of live loads (LL) as per Article 7.3.1 of SNI 1726:2019 which is 25% LL for storage areas. This mass is used in modal analysis to determine the period of vibration and in the calculation of seismic base shear force. The key parameters used in the determination of earthquake loads for this study are summarised in Table 8.

Table 9 EQ Determination Parameters

No	Earthquake Parameters	Value / Description	Reference
1	Location	Banyumas Regency, Central Java	PuSGeN Earthquake Map
2	Soil Site Class	SE (Soft Soil)	Table 5
3	Bedrock Acceleration (0.2s) (Ss)	0.7813	Picture 14-21
4	Site Coefficient (Short Period) (Fa)	0.3837	Picture 14-21
5	Site Coefficient (1 s period) (Fv)	1,27496	Table 6

No	Earthquake Parameters	Value / Description	Reference
6	Design Acceleration (0.2s) (SDS)	2,4652	Table 7
7	Design Acceleration (1.0s) (SD1)	0,6648 g	Equation (10)
8	Building Risk Category	0,6306 g	Equation (11)
9	Building Risk Category	IV	Table 3
10	Earthquake Vulnerability Factor (Ie)	1.50	Table 4
11	Seismic Design Category (KDS)	D	Table 8 & 9
12	Structure System	SRPMK Reinforced Concrete	Table 11
13	Response Modification Factor (R)	8	Table 12
14	System Overpower Factor (Ωo)	3	Table 12
15	Deflection Magnification Factor (Cd)	5.5	Table 12

2.4.5 Wind Load (WL)

Wind load (WL) is the lateral load acting on the external surfaces of a building due to the pressure and suction generated by the wind flow around the structure [47], [48]. This load is dynamic in nature and its magnitude depends on wind speed, building geometry, geographical location, surrounding environmental conditions (terrain roughness), and building height [49], [50], [51]. Wind load calculation is important to ensure the stability and strength of the structure against non-seismic lateral forces.

In this study, the calculation of wind forces acting on the structure was performed automatically using the wind load analysis feature of ETABS software version 22.5.1. The software implements wind load calculation procedures based on user-selected standards, in this case referring to the principles set out in SNI 1727:2020 (which adopts ASCE 7-16). To enable ETABS to automatically calculate wind loads, a series of key parameters need to be inputted by the user. These parameters define site-specific wind conditions and relevant building characteristics. The key parameters inputted into ETABS for wind load analysis in this study are summarised in Table 9.

Table 10 WL Input Parameters

No	Input Parameters	Symbol	Value / Description	References
1	Wind Loading Standard	Wind Load Code	ASCE 7-16 (As a reference principle for SNI 1727: 2020)	
2	Base Wind Speed (3-second)	Wind Speed (V)	39,9 m/s	Picture 26.5-1/2
3	Exposure Category		C	Article 26.7
4	Building Risk Category	-	IV	Table 1.5-1
5	Topographical Factors	Kzt	1.0	Article 26.8
6	Directionality Factor	Kd	0.85	Table 26.6-1
7	Wind Dynamic Effect Factor	Gust Effect Factor	ETABS auto-calculated	Article 26.11
8	Internal Pressure Coefficient	GCpi	±0.18 (Closed Building)	Article 26.11
9	Wind Load Application		Exposure from Shell Objects	-

By inputting the parameters in Table 12, ETABS can automatically generate wind loading cases from various directions and calculate the resulting lateral forces and torques on the structure for use in loading combinations.

2.5 Loading Combinations

2.5.1 Basic Load Combination

SNI 2847:2019 Article 5.3.1 specifies the basic load combination for strength design. These combinations generally consider gravity loads and environmental loads such as wind, but do not specifically include details of vertical earthquake effects or redundancy factors. The main basic combinations include (with D = Total Dead Load (DL+SDL), L = Floor Live Load, W = Wind Load):

1. 1.4 D
2. 1.2 D + 1.6 L
3. 1.2 D + 1.6 L + 0.5 W
4. 1.2 D + 1.0 W + 1.0 L
5. 0.9 D + 1.0 W

Kombinasi yang melibatkan beban gempa (E) dalam SNI 2847:2019 (misalnya 1.2 D + 1.0 E + 1.0 L) merujuk pada definisi E yang lebih rinci dalam SNI 1726:2019.

2.5.2 Load Combinations with Earthquake Effects (E)

SNI 1726:2019 Article 7.3.3 specifically defines the load combinations that should be used when taking into account the effects of earthquake loads (E) for strength design. The

definition of earthquake load effect (E) includes both horizontal and vertical components:

E = ϱ Eh ± Ev

where:

- ϱ = Redundancy factor, which depends on the Seismic Design Category (KDS). For structures in KDS D, E, or F, the value of ϱ is determined based on the evaluation of the structural resistance if the critical vertical elements are removed, but shall not be less than 1.3 (SNI 1726:2019 Article 7.3.4.1). In this study, with a KDS value of D for Banyumas Regency, the value of ϱ is 1.0.
- Eh = Horizontal earthquake force effect. For structures in KDS D, the effects of orthogonal earthquake loading must be taken into account (SNI 1726:2019 Article 7.5.4). This means that Eh is calculated as a combination of the effects of earthquakes in the two main directions (X and Y)
  Eh = ± (Ex + 0.3 Ey)
  Eh = ± (0.3 Ex + Ey)
- Ev = Vertical earthquake force effect, calculated using the formula:
  Ev = 0.2 * SDS * D (SNI 1726:2019 Pasal 7.3.3.1).
  SDS is the design acceleration spectral response parameter at short periods, and D is the total dead load (DL+SDL).

2.5.3 Required Strong Load Combination Formula (Seismic)

Based on the definition of E above and referring to SNI 1726:2019 Article 7.3.3, the main necessary force load combinations involving earthquake effects (including ϱ and SDS) and need to be defined or generated automatically in ETABS for structural element design are as follows (assuming ϱ = 1.3 and S = Snow Load = 0):

1. Combination of main earthquake load (maximum gravity)
   (1.2 + 0.2 SDS) D + ϱ Eh + 1.0 L
   Since Eh includes orthogonal effects and positivenegative directions, this combination is broken down into several specific load cases:
   - Combo 1a: (1.2 + 0.2 SDS) D + 1.0 (Ex + 0.3 Ey) + 1.0 L
   - Combo 1b: (1.2 + 0.2 SDS) D - 1.0 (Ex + 0.3 Ey) + 1.0 L
   - Combo 1c: (1.2 + 0.2 SDS) D + 1.0 (0.3 Ex + Ey) + 1.0 L
   - Combo 1d: (1.2 + 0.2 SDS) D - 1.0 (0.3 Ex + Ey) + 1.0 L
   - Combo 1e: (1.2 + 0.2 SDS) D + 1.0 (Ex - 0.3 Ey) + 1.0 L
   - Combo 1f: (1.2 + 0.2 SDS) D - 1.0 (Ex - 0.3 Ey) + 1.0 L
   - Combo 1g: (1.2 + 0.2 SDS) D + 1.0 (-0.3 Ex + Ey) + 1.0 L
   - Combo 1h: (1.2 + 0.2 SDS) D - 1.0 (-0.3 Ex + Ey) + 1.0 L
2. Combination of main earthquake loads (minimum gravity - uplift and stability checks)
   (0.9 - 0.2 SDS) D + ϱ Eh
   Similar to the first combination, this is elaborated based on Eh:
   - Combo 2a: (0.9 - 0.2 SDS) D + 1.0 (Ex + 0.3 Ey)
   - Combo 2b: (0.9 - 0.2 SDS) D - 1.0 (Ex + 0.3 Ey)
   - Combo 2c: (0.9 - 0.2 SDS) D + 1.0 (0.3 Ex + Ey)
   - Combo 2d: (0.9 - 0.2 SDS) D - 1.0 (0.3 Ex + Ey)
   - Combo 2e: (0.9 - 0.2 SDS) D + 1.0 (Ex - 0.3 Ey)
   - Combo 2f: (0.9 - 0.2 SDS) D - 1.0 (Ex - 0.3 Ey)
   - Combo 2g: (0.9 - 0.2 SDS) D + 1.0 (-0.3 Ex + Ey)
   - Combo 2h: (0.9 - 0.2 SDS) D - 1.0 (-0.3 Ex + Ey)

2.6 Analysis Model Matrix

The combination of three building height categories (LR, MR, HR) and five concrete grade variations (fc' = 20, 25, 30, 35, 40 MPa) resulted in a total of 15 unique structural analysis models. This analysis model matrix succinctly summarises the scope of the parametric study conducted and is presented in Table 10. Each cell in the table represents one analysed structural model.

Table 11 Analysis Model Matrix

Altitude Category	**fc' = 20 MPa**	**fc' = 25 MPa**	**fc' = 30 MPa**	**fc' = 35 MPa**	**fc' = 40 MPa**
LR (3 Floors)	LR-20	LR-25	LR-30	LR-35	LR-40
MR (6 Floors)	MR-20	MR-25	MR-30	MR-35	MR-40
HR (12 Floors)	HR-20	HR-25	HR-30	HR-35	HR-40

2.7 Analysis Procedure and Evaluated Output

For each of the 15 structural models, the following analysis procedures were performed using ETABS:

1. Modal analysis. This analysis was performed to determine the natural frequency (ω), natural vibrating period (T), and mode shape of the structure. Modal analysis is important to understand the basic dynamic characteristics of each model and as input for response spectrum analysis [52], [53].
2. Response Spectrum Analysis (RSA). RSA is the main analysis method used to determine the maximum seismic response of the structure to the plan earthquake represented by the design response spectrum as shown in Figure 4 [54], [55].
3. Consideration of the P-Delta Effect. The second-order effect (P-Delta), which is the interaction between the gravity load (P) and the lateral displacement (Δ) that can magnify the moment and displacement, is taken into account in the analysis [58], [59]. The P-Delta effect is included iteratively based on the specified gravity load combination, which is 1.0D + 0.25L. As per SNI 1726:2019 Article 7.8.7, the P-Delta effect shall be taken into account if the stability coefficient (θ) exceeds 0.10 [56]. In this study, the P-Delta effect was consistently included in all model analyses for accuracy, especially in the more flexible MR and HR models.

The main outputs evaluated from the analysis results for each model are:

- Fundamental Vibration Period (T1). The longest natural vibrating period of the structure, usually associated with the dominant translational mode.
- Maximum lateral deviation at the roof (δ_roof). The value of the largest lateral deviation occurring at the centre of mass of the roof floor, in the X and Y directions. This value is the result of elastic analysis (δxe) that has been multiplied by the deflection magnification factor (Cd) and divided by the earthquake primacy factor (Ie) according to SNI 1726:2019 Article 7.8.6, namely: $\delta x = \frac{(Cd)*(\delta xe)}{Ie}$
- Inter-Story Drift Rasio (IDR)
  Inter-Story Drift Ratio (IDR). IDR is calculated for each level (i) as the difference in lateral deviation between floor i and the floor below it (i-1), divided by the height of that

floor (hsx):

$IDRi = \frac{\delta_{xi} - \delta_{x(i-1)}}{hsxi}$

The reported IDR value is also the value that has been multiplied by Cd/Ie.

- Maximum IDR (IDRmax), which is the largest IDR value that occurred among all levels in the building, along with identification of the floor number where the IDRmax occurred.
- IDR distribution profile, a graph plotting IDR values against floor number or building height, to visualise deformation patterns between levels along the height of the structure.

3. Result and Discussion

3.1 Presentation of Results

3.1.1 Fundamental Vibration Period (T1)

The natural vibration period of the structure, especially the fundamental period (T1) associated with the first vibration mode, is a crucial parameter that reflects the inherent flexibility of the structure. Tables 11, 12 and 13 present the natural period of vibration for the first 12 modes in all 15 analysis models.

Table 12 Fundamental Period (T1) for HR Model

Model ID	HR-20	HR-25	HR-30	HR-35	HR-40
Mode 1	4,178	3,952	3,776	3,633	3,514
Mode 2	3,141	2,97	2,838	2,731	2,641
Mode 3	2,791	2,64	2,522	2,427	2,347
Mode 4	1,347	1,274	1,218	1,172	1,133
Mode 5	1,025	0,969	0,926	0,891	0,862
Mode 6	0,919	0,869	0,83	0,799	0,773
Mode 7	0,761	0,719	0,687	0,661	0,64
Mode 8	0,591	0,559	0,534	0,514	0,497
Mode 9	0,537	0,508	0,485	0,467	0,452
Mode 10	0,505	0,478	0,457	0,439	0,425
Mode 11	0,401	0,379	0,362	0,348	0,337
Mode 12	0,373	0,353	0,337	0,325	0,314

Table 13 Fundamental Period (T1) for MR Model

Model ID	MR-20	MR-25	MR-30	MR-35	MR-40
Mode 1	2,058	1,947	1,86	1,79	1,731
Mode 2	1,578	1,492	1,426	1,372	1,327
Mode 3	1,412	1,335	1,276	1,228	1,187
Mode 4	0,63	0,596	0,569	0,548	0,53
Mode 5	0,494	0,467	0,446	0,43	0,415
Mode 6	0,454	0,429	0,41	0,395	0,382
Mode 7	0,33	0,312	0,298	0,287	0,278
Mode 8	0,268	0,253	0,242	0,233	0,225
Mode 9	0,257	0,243	0,232	0,223	0,216
Mode 10	0,205	0,194	0,185	0,178	0,172
Mode 11	0,173	0,163	0,156	0,15	0,145
Mode 12	0,171	0,162	0,155	0,149	0,144

Table 14 Fundamental Period (T1) for LR Model

Model ID	LR-20	LR-25	LR-30	LR-35	LR-40
Mode 1	1,005	0,951	0,908	0,874	0,845
Mode 2	0,789	0,747	0,713	0,686	0,664
Mode 3	0,721	0,681	0,651	0,626	0,606
Mode 4	0,293	0,277	0,264	0,254	0,246
Mode 5	0,241	0,228	0,218	0,209	0,202
Mode 6	0,234	0,221	0,211	0,203	0,197
Mode 7	0,145	0,137	0,131	0,126	0,122
Mode 8	0,131	0,124	0,118	0,114	0,11
Mode 9	0,124	0,117	0,112	0,108	0,104
Mode 10	0,069	0,065	0,062	0,06	0,058
Mode 11	0,065	0,061	0,059	0,056	0,055
Mode 12	0,06	0,056	0,054	0,052	0,05

The natural vibration period data presented in Tables 16, 17, and 18 consistently show a significant trend: increasing the concrete grade (fc') from 20 MPa to 40 MPa systematically results in a decrease in vibration period (T) values for all observed modes, across all three height categories (HR, MR, LR). Focusing on the fundamental period (T1), in the tall building (HR, Table 16), T1 was reduced from 4.178 seconds at fc'=20 MPa to 3.514 seconds at fc'=40 MPa, or a decrease of about 15.9%. In the mid building (MR, Table 17), T1 was reduced from 2,058 seconds (fc'=20 MPa) to 1,731 seconds (fc'=40 MPa), a decrease of about 15.9%. While in the low building (LR, Table 18), T1 was reduced from 1.005 seconds (fc'=20 MPa) to 0.845 seconds (fc'=40 MPa), a decrease of about 15.9%.

This trend of period reduction is not only limited to T1, but is also observed in the periods of higher modes (T2, T3, etc.). For example, T2 in the HR model decreased from 3.141 s to 2.641 s when fc' increased from 20 to 40 MPa. The same pattern is seen for the other modes in Tables 16, 17, and 18. This decrease in the overall natural vibration period directly indicates an increase in the stiffness (k) of the structure as the concrete grade (fc') increases, in accordance with the basic theoretical relationship $T = (2)*(\pi)*(\frac{m}{k})$.

To visualise the relationship between concrete grade and fundamental period more clearly, the T1 data from Tables 11, 12, and 13 are plotted against the variation of fc' for each height category in Figures 8, 9, and 10 below.

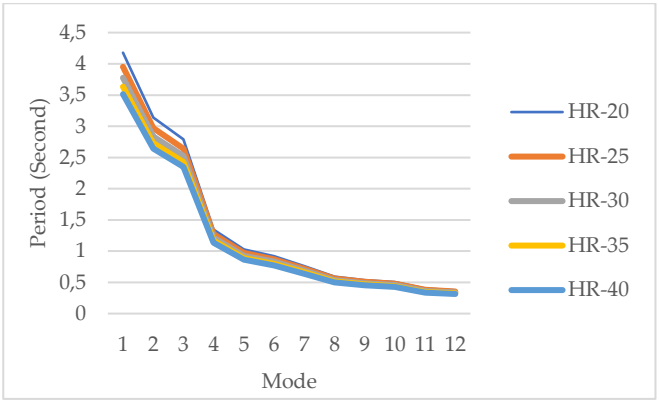

Figure 8 Relationship between Concrete Quality (fc') and Fundamental Period (T1) in High-Rise Building

The graph in Figure 8 plots T1 (Y-axis, in seconds) against fc' (X-axis, in MPa) for the tall building (HR) model. It is clear that T1 decreases as fc' increases. The curve tends to slope at higher values of fc', indicating that the sensitivity of T1 to changes in fc' decreases at higher concrete grades. For example, the decrease in T1 from fc' 20 to 25 MPa is greater than the decrease in T1 from fc' 35 to 40 MPa.

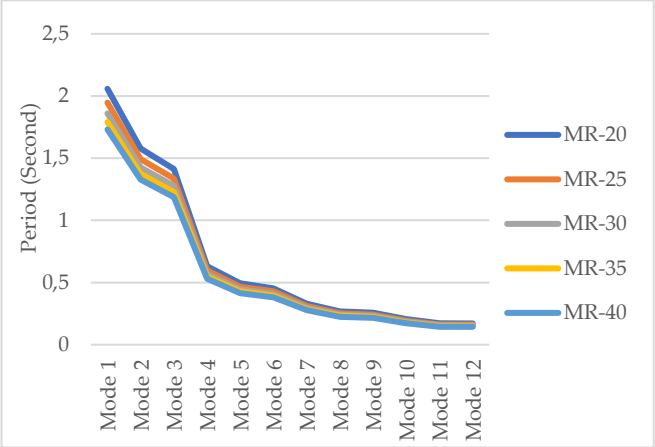

Figure 9 Relationship between Concrete Quality (fc') and Fundamental Period (T1) of Mid-Rise Building

The graph in Figure 9 presents a similar relationship between T1 and fc' for the mid building model (MR). The pattern of decreasing T1 with increasing fc' is also clearly observed. Just like in the HR building, the curves show a non-linear relationship, where the decrease in T1 becomes less significant at higher fc' ranges.

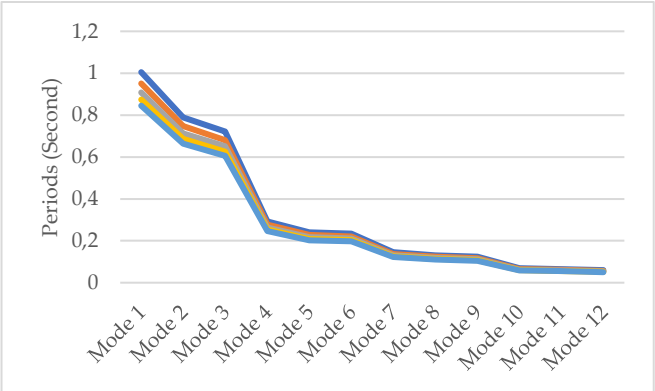

Figure 10 Relationship between Concrete Quality (fc') and Fundamental Period (T1) in Low-Rise Building

This graph in Figure 10 for the low-rise (LR) building again confirms the same trend. T1 decreases consistently with increasing fc', and the relationship is non-linear with decreasing sensitivity at high fc'. A visual comparison between Figures 14, 15 and 16 also shows significant absolute differences in T1 values between height categories, as expected with taller buildings having longer fundamental periods.

3.1.2 Maximum Lateral Deviation at Roof (δroof)

The maximum lateral deviation at roof (δroof) is a measure of the global displacement response of the structure to earthquake loads. Table 14 presents the δroof values (in mm, after multiplying by the factor Cd/Ie = 5.5/1.5) for the X direction (critical direction) in all 15 analysis models.

Table 15 Maximum Lateral Deviation at Roof (δroof, mm)

fc' (MPa)	δroof - LR (3 Lt)	δroof - MR (6 Lt)	δroof - HR (12 Lt)
20	26,672	57,221	127,883
25	25,094	51,18	114,382
30	22,553	46,721	104,416
35	21,101	43,256	96,672
40	19,682	40,462	90,428

The data in Table 14 show a clear trend: increasing the concrete grade (fc') consistently reduces the maximum lateral deviation at the roof (δroof) across all building height categories. For example, in high-rise buildings (HR), δroof is reduced from 127.883 mm (fc'=20 MPa) to 90.428 mm (fc'=40 MPa), or a reduction of 29.3%. In mid buildings (MR), the reduction is from 57,221 mm to 40,462 mm (29.3% reduction), and in low buildings (LR), from 26,672 mm to 19,682 mm (26.2% reduction). This reduction in deviation is a direct consequence of the increase in structural stiffness due to the increase in fc' and Ec. A stiffer structure has greater resistance to lateral deformation due to earthquake forces. In addition, it is clear that the height of the building has a dominant influence on the magnitude of the deviation; taller buildings experience significantly greater roof deviation than lower buildings for the same concrete quality.

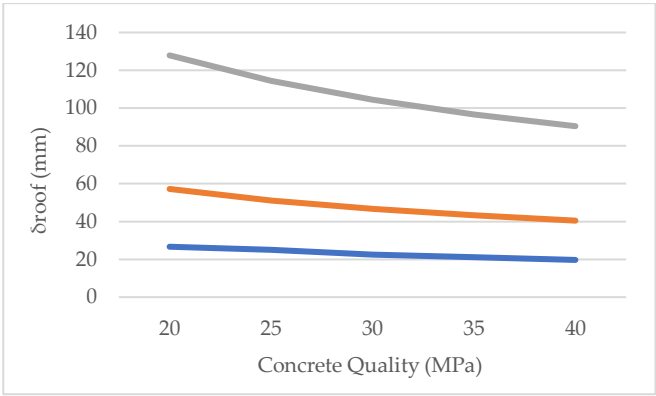

Figure 11 Comparison of Maximum Lateral Deviation at Roof (δroof) for Different Concrete Quality and Building Height

3.1.3 Maximum Interlevel Deviation Ratio (IDRmax)

The interlevel deviation ratio (IDR) is a critical parameter that measures the relative deformation between successive floors and is directly related to potential damage to structural and non-structural elements. IDRmax is the largest IDR value that occurs along the building height. Table 15 presents the IDRmax value (in per cent, after multiplying by the Cd/Ie factor), the floor where the IDRmax occurs, and its comparison with the SNI 1726:2019 clearance limit (Δa = 0.015 or 1.5% of level height, hsx) for risk category IV buildings with SRPMK..

Table 16 Maximum inter-storey deviation ratio (IDRmax)

Model	IDRmax (%)	Floor Occurs	Limit SNI (%)	Status
LR-20	19,69056	3	1.5	NOT OK
LR-25	19,69056	3	1.5	NOT OK

Model	IDRmax (%)	Floor Occurs	Limit SNI (%)	Status
LR-30	19,69056	3	1.5	NOT OK
LR-35	19,69056	3	1.5	NOT OK
LR-40	19,69056	3	1.5	NOT OK
MR-20	8,66662	4	1.5	NOT OK
MR-25	8,66662	4	1.5	NOT OK
MR-30	8,66662	4	1.5	NOT OK
MR-35	8,66662	4	1.5	NOT OK
MR-40	8,66662	4	1.5	NOT OK
HR-20	5,0195	11	1.5	NOT OK
HR-25	5,0195	11	1.5	NOT OK
HR-30	5,0195	11	1.5	NOT OK
HR-35	5,0195	11	1.5	NOT OK
HR-40	5,0195	11	1.5	NOT OK

Similar to the trend in roof deviation, the IDRmax values also show a consistent decrease as the concrete grade (fc') increases across all height categories. Based on the interpretation of the data, the total reduction of IDRmax from fc'=20 MPa to fc'=40 MPa is about 21.3% for low buildings (LR), 19.3% for mid buildings (MR), and 18.8% for high buildings (HR). This decrease once again confirms that the increased stiffness due to the higher concrete grade is effective in controlling the deformation between levels, which is crucial for limiting damage.

Another interesting aspect revealed from Table 15 is the change in the location (floor) of IDRmax occurrence as the building height changes. In low-rise buildings (LR), IDRmax consistently occurs at the top floor (Floor 3). This is a typical pattern for low structures whose dynamic response tends to be dominated by the first vibration mode and shear-type behaviour, where the largest deformations are concentrated at the top. However, in the mid (MR) and high (HR) buildings, the location of IDRmax shifts downwards, i.e. to the upper-middle floors (Floor 4 for MR and Floor 11 for HR). This shift in IDRmax location indicates a change in the dynamic behaviour of the structure. In taller buildings, the influence of higher vibration modes becomes more significant, and global flexural-type behaviour begins to dominate. This combination of effects causes the largest concentration of inter-level deformation to occur not at the roof, but around the middle to three-quarters of the building height.

Evaluation of the SNI 1726:2019 inter-level deformation limit criteria (Δa = 1.5% hsx) showed critical results. Based on the reinterpreted IDRmax values in Table 15, most models (11 out of 15) do not fulfil this permit limit. Only the high building model with the highest concrete grade (HR-35 and HR-40) and the mid building model with the highest concrete grade (MR-40, whose value is right at the limit) fulfil the drift requirement. The low building model (LR) did not fulfil the permit limit even at fc'=40 MPa. This finding has significant design implications: for the structural geometry configuration and seismic loading level analysed (Banyumas site, KDS D), increasing the concrete grade to 40 MPa is not sufficient to ensure compliance with the inter-level deviation limit requirements of SNI 1726:2019 in the majority of cases.

3.1.4 IDR Distribution Profiles

To gain a more comprehensive understanding of the deformation pattern along the building height, IDR distribution profiles (IDR values at each level) were plotted for each height category, comparing the effect of fc' variation. Figures 12, 13, and 14 present these profiles.

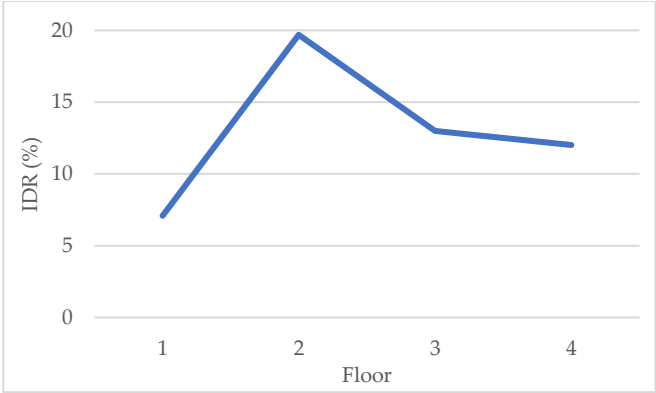

Figure 12 IDR Distribution Profile Along Low Building Height (LR)

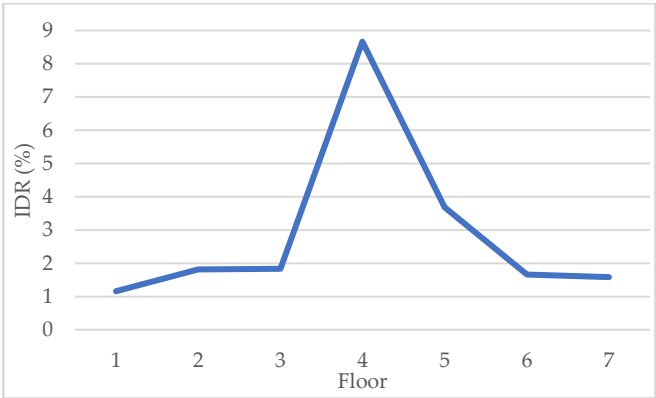

Figure 13 IDR Distribution Profile Along Mid Building Height (MR)

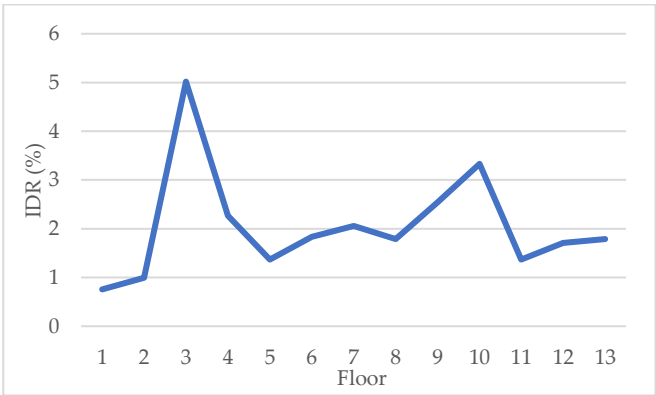

Figure 14 IDR Distribution Profile Along the Height of Tall Buildings (HR)

Figure 12 (Low Building - LR) shows an IDR profile that tends to increase monotonically from the ground floor to reach a maximum value at the top floor (Floor 3). This profile

shape is consistent with the shear dominant behaviour common in low-rise buildings. An increase in fc' (from fc'20 to fc'40 curves) clearly decreases the overall profile curve, indicating a reduction in IDR at all levels, but the basic shape of the profile remains relatively unchanged.

Figure 13 (Mid Building - MR) displays the IDR profile with a different shape. The IDR value increases from the base, reaches a peak at the middle floor (Floor 4), and then decreases slightly towards the roof. This convex shape reflects the combination of shear and flexural behaviour, as well as the onset of the influence of higher vibration modes. Again, increasing fc' consistently decreases the IDR magnitude at all levels, shifting the entire curve downwards.

Figure 14 (Tall Buildings - HR) shows the IDR profile increasingly accentuating flexural behaviour and high mode effects. The IDR increases sharply in the lower floors, reaches a maximum value in the upper-middle floor (Floor 11), and then decreases significantly towards the roof. This 'bulging' profile shape in the upper-middle section is characteristic of flexible tall buildings. The increase in fc' again shows a global IDR-reducing effect across the building height, but the basic distribution pattern is maintained.

Overall, this IDR profile not only confirms the IDRmax locations identified in Table 15, but also provides a clear visual illustration of how the deformation pattern between levels changes significantly as the building height increases, as well as how the increase in concrete grade consistently reduces the deformation level across heights.

3.2 Discussion

3.2.1 Effect of Increasing fc' on Deformation

The analytical results consistently show that increasing the concrete compressive strength grade (fc') has a significant and beneficial effect on reducing the seismic deformation response of reinforced concrete buildings. An increase in fc' directly increases the modulus of elasticity of concrete (Ec), which in turn increases the flexural stiffness (EI) and shear stiffness (GA) of structural elements (columns, beams, slabs). This increase in element stiffness leads to an increase in the overall stiffness of the structure, which results in a shorter natural vibration period (Tables 11-13, Figures 8-10) as well as a decrease in the maximum lateral deviation at the roof (δroof) and the maximum inter-level deviation ratio (IDRmax) (Tables 14, 15, Figures 11-14). To quantify these effects in more detail, Table 16 presents the percentage reduction in deformation (δroof and IDRmax) for each 5 MPa increase in fc' interval, from 20 MPa to 40 MPa.

Table 17 Quantification of Deformation Reduction Percentage Due to Increase in fc'

Category	Parameter	Interval fc' (MPa)	% Reduction
LR (3 Lt)	δroof	20 -> 25	5.92%
		25 -> 30	10.13%
		30 -> 35	6.44%
		35 -> 40	6.72%
	IDRmax	20 -> 40	~21.3%
MR (6 Lt)	δroof	20 -> 25	10.56%
		25 -> 30	8.71%
		30 -> 35	7.42%
		35 -> 40	6.46%
	IDRmax	20 -> 40	~19.3%
HR (12 Lt)	δroof	20 -> 25	10.56%
		25 -> 30	8.71%
		30 -> 35	7.42%
		35 -> 40	6.46%
	IDRmax	20 -> 40	~18.8%

The quantitative data in Table 16 show that although increasing fc' always results in deformation reduction, the effectiveness of increasing fc' tends to decrease at higher concrete grade ranges. For example, in MR and HR buildings, an increase in fc' from 20 to 25 MPa gives a reduction in δroof of about 10.6%, while an increase from 35 to 40 MPa only gives a reduction of about 6.5%. This phenomenon of diminishing returns is consistent with the non-linear relationship between fc' and Ec ($Ec \propto \sqrt{fc}$) and the observations on the T1 vs fc' curves (Figures 8-10). The total reduction of δroof as fc' increases from 20 to 40 MPa ranges from 26.2% (LR) to 29.3% (MR & HR), while the total reduction of IDRmax ranges from 18.8% (HR) to 21.3% (LR).

These reduction magnitudes suggest that concrete grade is an effective design parameter for controlling seismic deviation. However, a crucial finding of this study is that for the specific building configurations and seismic loads analysed (Banyumas site, KDS D, SRPMK), increasing fc' to 40 MPa alone proved insufficient to meet the SNI 1726:2019 allowable inter-level deviation limit (1.5%) in most cases, especially for low- and mid-rise buildings. This implies that drift control strategies require a combination of material upgrades with dimensional adjustments of structural elements or the addition of other stiffness elements (such as shear walls).

3.2.2 Effect of Building Height on Deformation Patterns

This study clearly shows that the building height fundamentally affects both the magnitude and distribution pattern of seismic deformations. As expected, the total lateral deviation (δroof) increases significantly with increasing building height (Table 14, Figure 11), as taller structures are generally more flexible (have longer T1, see Tables 11-13) and accumulate larger displacements at the apex.

However, the more interesting influence is on the inter-level deformation pattern (IDR). The IDR distribution profiles (Figures 12-14) show a clear transition in behaviour as height increases. Low-rise buildings (LR) show an IDR profile dominated by the first vibrating mode with shear-type behaviour, where the largest IDR occurs at the top floor. In contrast, mid-rise (MR) and especially high-rise (HR) buildings show IDR profiles influenced by higher vibration modes and global flexural-type behaviour. In these cases, the largest IDRmax no longer occurs at the roof, but shifts to the floors below (4th floor for MR, 11th floor for HR).

This shift in IDRmax location has important implications in design, as it shows that the critical floors that experience the largest deformation demand change depending on the height and flexibility of the structure. Understanding this IDR distribution pattern is crucial for identifying potential damage locations and focusing the details of the ductile reinforcement. An interaction between concrete grade and height is also observed; although increasing fc' always reduces deformation, the sensitivity of IDRmax reduction appears to differ slightly between heights (LR experiences the largest

total IDRmax reduction of 21.3%, compared to HR's 18.8%), suggesting that the effectiveness of increasing fc′ in controlling drift is slightly influenced by the dominant dynamic behaviour (shear vs. flexure) associated with deformation.

3.2.3 Comparison with Other Studies and Unique Contributions

The findings of this study are in line with the general conclusions of previous studies showing that the use of higher grade concrete (fc') tends to increase structural stiffness, shorten the vibration period, and reduce lateral deviation and IDR. For example, studies by [24], [25], [57], [58] also found that the use of different grade concrete affects the level stiffness, period, and deviation in multi-storey buildings. Similarly, the importance of IDR as a damage indicator and the influence of height on IDR patterns (including the shift in IDRmax location and the influence of higher modes) have been widely discussed in the literature.

However, the unique contribution of this study lies in its methodological approach that isolates specifically the effect of fc' variations (from 20 to 40 MPa) by keeping the typical plan geometry and dimensions of all structural elements (columns, beams, slabs) constant across all three height categories (LR, MR, HR). This controlled parametric approach allows a purer quantification of the sensitivity of the seismic deformation response (δroof, IDRmax, IDR profile) to changes in the material properties of the concrete itself, without being distorted by simultaneous changes in element dimensions that often occur in design or optimisation studies. The ability to map the influence of fc' directly on different levels of dynamic complexity (represented by LR, MR, HR) provides a deeper understanding of the interaction between material properties and the global dynamic characteristics of the structure.

Another significant finding is the quantitative demonstration that in the context of SNI 1726:2019 for seismically active locations (KDS D) and SRPMK structural systems, increasing the concrete grade to 40 MPa does not necessarily guarantee the fulfilment of the inter-level clearance deviation limit (1.5%). This highlights the importance of careful drift evaluation in the design process and demonstrates that reliance solely on material upgrades is inadequate as a single strategy for drift control in certain cases.

4. Conclusion

Based on the results of the parametric analysis and discussion that has been carried out, the following conclusions can be drawn:

1. Increasing the concrete compressive strength (fc') from 20 MPa to 40 MPa consistently and significantly increases the stiffness of reinforced concrete structures. This is evidenced by the decrease in the fundamental natural vibrating period (T1) by about 15.9% for all height categories (LR, MR, HR). This increase in stiffness directly reduces the seismic deformation response, with reductions in maximum lateral deviation at the roof (δroof) ranging from 26.2% to 29.3% and reductions in maximum inter-level deviation ratio (IDRmax) ranging from 18.8% to 21.3% when fc' is increased from 20 to 40 MPa. The effect of these reductions is non-linear, with the effectiveness of increasing fc' tending to decrease at higher grades.
2. Building height fundamentally affects seismic deformation response. Taller structures exhibit significantly larger total lateral deviations (δroof). More importantly, the height changes the distribution pattern of the inter-level deviation (IDR) along the structure. In low-rise (LR) buildings, IDRmax occurs at the top floor, reflecting shear-dominant behaviour. In mid (MR) and high (HR) buildings, the location of IDRmax shifts to the middle-upper floors (4th floor for MR, 11th floor for HR), indicating a transition to flexural dominant behaviour and the influence of higher vibration modes.
3. Increasing fc' effectively reduces deformations at all height levels, but different IDR distribution patterns are maintained according to building height. There is an indication that the sensitivity of drift reduction (IDRmax) to the increase in fc' is slightly affected by the building height.
4. For the analysed structural geometry configuration (taken from the reference building), SRPMK structural system, and plan earthquake conditions for the Banyumas site (KDS D), increasing the concrete grade (fc') to 40 MPa alone proved insufficient to meet the SNI 1726:2019 interlevel drift limit requirement (1.5%) for most of the models, especially the low- and mid-rise buildings.

This research contributes a quantifiable quantification of the intrinsic influence of concrete grade on the seismic response of buildings of different heights, under controlled element geometry conditions. The findings confirm the important role of concrete grade in seismic performance, but also highlight the limits of its effectiveness as a single strategy to fulfil drift criteria under specific seismic conditions and structural configurations..

5. Suggestion

Based on the findings and limitations of this study, some suggestions for future research are as follows:

1. Conduct analysis with a wider range of fc' variations, including very high strength concrete (fc' > 50 MPa), to evaluate if the diminishing returns trend continues or if different behaviours emerge. In addition, varying other material parameters such as reinforcing steel grade (fy) may provide a more comprehensive picture.
2. Repeating the parametric study on different building plans (e.g., horizontally or vertically irregular) and different structural systems (e.g., shear wall-frame system, double system) to assess whether the effects of fc' and height are consistent in other configurations.
3. Using Non-Linear Time History Analysis (NLTHA) with various actual earthquake records to gain a deeper understanding of the structure's inelastic response, damage distribution, and more realistic performance evaluation than the elastic response spectrum method.
4. Include the effects of Soil-Structure Interaction (SSI) in the modelling, especially for tall buildings or those standing on soft soils (such as the SE site class used in this study), as SSI can affect the vibration period and deviation response of the structure.
5. Investigate design optimisation strategies that combine the use of different concrete grades with dimensional adjustments of structural elements (e.g. graded concrete or

column and beam size adjustments) to achieve seismic performance targets (including meeting drift limits) more efficiently and economically.

Conduct similar analyses for geographical locations with different seismicity levels and response spectrum characteristics to generalise the findings or identify the dependence of response on site-specific earthquake characteristics.

Acknowledgements

In the acknowledgment section, the author can state the source of research funding and, more specifically, the contract number. Make sure the statement complies with the guidelines provided by the funding agency. The author can also thank reviewers and proofreaders, technicians who help prepare equipment set-ups, or students who assist in surveys.

Author Declaration

Authors' contributions and responsibilities

The authors made substantial contributions to the conception and design of the study. The authors took responsibility for data analysis, interpretation, and discussion of results. The authors read and approved the final manuscript.

Availability of data and materials

All data are available from the authors.

Competing interests

The authors declare no competing interest.

References

[1] M. Rajif and Syafriani, "Hazard Seismic Zonation Analysis of West Sumatra Region using Probabilistic Hazard Seismic Analysis (PHSA) Method," *Pillar of Physics: Jurnal Berkala Ilmiah Fisika*, vol. 14, no. 1, 2021, doi: 10.24036/10753171074.

[2] N. T. Puspito *et al*., "Evaluation of Station Performance of the Indonesian Seismic Network Using the Primary Location Parameter," *Seismological Research Letters*, vol. 95, no. 2A, pp. 804–819, Mar. 2024, doi: https://doi.org/10.1785/0220220334.

[3] A. Y. A. Amira, Krisnamurtia, and K. A. Wiswamitra, "Comparison of Behavior of Reinforced Concrete Dual-system Structure (Frame-Shear Wall) and Steel Dual-system Structure (Frame- Special Plate Shear Wall) in High Rise Building (Case Study: IT Mandiri Bumi Slipi Building)," *Rekayasa Sipil*, vol. 18, no. 3, pp. 272–280, Sep. 2024, doi: 10.21776/ub.rekayasasipil.2024.018.03.13.

[4] H. Herman, D. Capry, G. Vitri, and W. P. Zayu, "Desain Ulang Struktur Bangunan Gedung Hotel Ibis Padang Dengan Tinjauan Fixed Base," *Jurnal Hasil Penelitian dan Pengkajian Ilmiah Eksakta*, vol. 1, no. 1, pp. 26–39, Jan. 2022, doi: 10.47233/jppie.v1i1.400.

[5] B. Liu, "Monitoring Algorithm for Lateral Displacement of Reinforced Concrete in Super High-rise Building," in *AIAM2021: 2021 3rd International Conference on Artificial Intelligence and Advanced Manufacture*, New York, NY, USA: Association for Computing Machinery, 2022, pp. 1549–1553. doi: 10.1145/3495018.3495438.

[6] D. Zebua and L. S. B. Wibowo, "Effect of Soil Type on Lateral Displacement of Reinforced Concrete Building," *Resilience in Construction*, vol. 3, no. 3, Oct. 2022, doi: 10.32722/arcee.v3i03.4965.

[7] Z. Peng, Z. Guo, Y. Shen, and X. Wang, "Inter-Story Drift Ratio Detection of High-Rise Buildings Based on Ambient Noise Recordings," *Appl. Sci.*, vol. 13, no. 11, p. 6724, May 2023, doi: 10.3390/app13116724.

[8] A. Sapre and R. Sinha, "Influence of Variation of Material Properties on Interstorey Drift of RC Frame Buildings," in *Recent Advances in Structural Engineering, Volume 2. Lecture Notes in Civil Engineering , vol 12.*, Springer: Singapore, 2019, pp. 609–622. doi: 10.1007/978-981-13-0365-4_52.

[9] H. Çolak, H. T. Türker, and H. Coşkun, "Accurate Estimation of Inter-Story Drift Ratio in Multistory Framed Buildings Using a Novel Continuous Beam Model," *Appl. Sci.*, vol. 13, no. 13, p. 7819, Jul. 2023, doi: 10.3390/app13137819.

[10] F. Wang, Q.-X. Shi, and P. Wang, "Research on the Physical Inter-story Drift Ratio and the Damage Evaluation of RC Shear Wall Structures," *KSCE Journal of Civil Engineering*, vol. 25, no. 6, pp. 2121–2133, Jun. 2021, doi: 10.1007/s12205-021-1486-7.

[11] SNI 1726-2019, "Tata Cara Perencanaan Ketahanan Gempa untuk Struktur bangunan gedung dan non gedung (Koreksi)," 2019, *Badan Standardisasi Nasional*.

[12] ACI 318, "ACI 318RM-14 Commentary on Building Code Requirements for Structural Concrete," 2014, *Farmington Hills, MI*.

[13] ACI 318-19, "Building Code Requirements for Structural Concrete (ACI 318-19)," 2019, *Farmington Hills, MI*.

[14] E. T. Tunc, "Variation of Dynamic Elasticity Modulus with Experimentally Determined Concrete Compressive Strength," *DUJE*, vol. 14, no. 4, pp. 761–766, Dec. 2023, doi: 10.24012/dumf.1365518.

[15] V. Revilla-Cuesta, R. Serrano-López, A. B. Espinosa, V. Ortega-López, and M. Skaf, "Analyzing the Relationship between Compressive Strength and Modulus of Elasticity in Concrete with Ladle Furnace Slag," *Buildings*, vol. 13, no. 12, p. 3100, Dec. 2023, doi: 10.3390/buildings13123100.

[16] W. L. A. Sabila, H. R. Husni, Bayzoni, and M. Isneini, "Evaluasi Kinerja Struktur Gedung Bertingkat dengan Metode Analisis Respon Spektrum (Studi Kasus: Gedung 5 Rumah Sakit Pendidikan Perguruan Tinggi Negeri (RSPTN) Universitas Lampung)," *Jurnal Rekayasa Sipil dan Desain (JRSDD)*, vol. 11, no. 3, pp. 493–504, Sep. 2023, doi: https://journal.eng.unila.ac.id/index.php/jrsdd/article/view/3532.

[17] R. W. Sun and G. C. Fanourakis, "An Assessment of Factors Affecting the Elastic Modulus of Concrete," *Structural Concrete*, vol. 23, no. 1, pp. 593–603, Feb. 2021, doi: 10.1002/suco.202000553.

[18] E. Alotaibi, M. Alhalabi, O. Mostafa, and S. Barakat, "Prediction of Concrete Modulus of Elasticity Using Deep Learning," *Advances in Science and Technology*, vol. 129, pp. 29–36, Aug. 2023, doi: 10.4028/p-nQs5bX.

[19] E. A. Ohemeng, A. Naghizadeh, and M. S. Ramabodu, "Empirical Model for Predicting Elastic Modulus of CRCA Concrete: An Approach towards Sustainable Concrete Design," *Advances in Science and Technology*, vol. 145, pp. 87–96, Mar. 2024, doi: 10.4028/p-yOR735.

[20] M. Cimesa and M. A. Moustafa, "UHPC Modulus of Elasticity: Assessment and New Developments using Companion Materials and Structural Data," *Eng Struct*, vol. 310, no. 118146, Jul. 2024, doi: 10.1016/j.engstruct.2024.118146.

[21] A. I. A. Momin, R. B. Khadiranaikar, and A. A. Zende, "Modulus of Elasticity of High-Performance Concrete Beams Under Flexure-Experimental Approach," in *Recent Trends in Construction Technology and Management. Lecture Notes in Civil Engineering, vol 260*, M. S. Ranadive, B. B. Das, Y. A. Mehta, and R. Gupta, Eds., Singapore: Springer, Sep. 2022, pp. 57–69.

[22] A. E. Mohamed, "Non-Linear Effect on Flexural Stiffness of Reinforced Concrete Rectangular Sections," *International Journal of Advanced Engineering and Business Sciences*, vol. 5, no. 1, pp. 22–38, Feb. 2024, doi: 10.21608/ijaebs.2024.266205.1091.

[23] C.-H. Chin, M.-Y. Cheng, A. Lepage, and R. D. Lequesne, "Shake Table Tests to Compare the Seismic Response of Concrete Frames with Conventional and High-Strength Reinforcement," *Earthq Eng Struct Dyn*, vol. 53, no. 1, pp. 89–115, Jan. 2024, doi: 10.1002/eqe.4008.

[24] Hakas Prayuda *et al.*, "Effect of Different Grades of Concrete on RC Framed Multi Storied Building," in *IOP Conference Series: Materials Science and Engineering, Volume 1144, 3rd International Symposium on Civil and Environmental Engineering (ISCEE 2020)*, Batu Pahat,Johor, Malaysia: IOP Publishing Ltd, Dec. 2020. doi: 10.1088/1757-899X/1144/1/012014.

[25] V. Ramesh and C. Raju, "Effect of Different Grades of Concrete on RC Framed Multi Storied Building," *E3S Web of Conferences*, vol. 309, no. 01194, 2021, doi: https://doi.org/10.1051/e3sconf/202130901194.

[26] Z.-N. Wu *et al.*, "Seismic Intensity Measure Selection Incorporating Interaction Effects for Damage Assessment Across Different Structural Sensitive Regions," *Structures*, vol. 67, no. 106917, Sep. 2024, doi: 10.1016/j.istruc.2024.106917.

[27] Y. Yan, Y. Xia, and L. Sun, "Efficient Sensitivity Analysis for Structural Seismic Fragility Assessment Based on Surrogate Models," *Structures*, vol. 69, no. 107299, Nov. 2024, doi: 10.1016/j.istruc.2024.107299.

[28] B. A. Rahman and K. Galal, "Sensitivity of the Seismic Response of Reinforced Concrete Masonry Walls with Boundary Elements to Design Parameters," *Eng Struct*, vol. 255, no. 113953, Mar. 2022, doi: 10.1016/j.engstruct.2022.113953.

[29] A. Foyouzati and A. Khaloo, "Seismic Performance Assessment and Fragility Analysis of Concrete Structures Equipped with Self-Centered Hybrid Wall Systems," *Sustain Resilient Infrastruct*, vol. 10, no. 2, pp. 147–165, Sep. 2024, doi: 10.1080/23789689.2024.2403866.

[30] M. Derife, A. Atmani, E. H. A. Laasri, J. Balil, and D. Agliz, "Development of a Low Cost System for Modal Parameters Identification under Ambient Vibration: A Low Rise Building as a Case Study," *Journal of Building Engineering*, vol. 54, no. 104626, Aug. 2022, doi: 10.1016/j.jobe.2022.104626.

[31] J. Bai, J. Zhang, K. Du, and S. Jin, "A Simplified Seismic Design Method for Low-Rise Dual Frame-Steel Plate Shear Wall Structures," *Steel and Composite Structures*, vol. 37, no. 4, pp. 447–462, Nov. 2020, doi: 10.12989/scs.2020.37.4.447.

[32] G. Diaz-Martinez and A. Teran-Gilmore, "Prediction of the Influence of Higher Modes on the Dynamic Response of High-Rise Buildings Subjected to Narrow-Banded Ground Motions," *International Journal of Structural Stability and Dynamics*, vol. 23, no. 4, p. 2350114, 2023, doi: 10.1142/S0219455423501146.

[33] F. Tong and C. Christopoulos, "Insights on Higher-Mode Effects in High-Rise Buildings with Flexible Base Rotational and Translational Restraints: A Theoretical Study Using a Continuum Beam Analogy," *Journal of Earthquake Engineering*, vol. 27, no. 2, pp. 314–339, Dec. 2021, doi: 10.1080/13632469.2021.2001394.

[34] A. Kumar, Shantnu, and O. Sharad, "A Study on the Variations in Lateral Loading Imapcats Between Medium and High-rise Buildings Under Diverse Enviromental Conditions," *International Journal For Multidisciplinary Research*, vol. 6, no. 2, Apr. 2024, doi: 10.36948/ijfmr.2024.v06i02.16142.

[35] A. Kumar, Shantnu, and O. Sharad, "A Study on the Variations in Lateral Loading Imapcats Between Medium and High-rise Buildings Under Diverse Enviromental Conditions," *International Journal For Multidisciplinary Research*, vol. 6, no. 2, Apr. 2024.

[36] R. Saharia, D. Bhuyan, S. Chowdhury, and K. Bharadwaj, "Comparative Study on Static and Dynamic Analysis of RC Buildings of Different Heights in Different Seismic Zones," in *Recent Advances in Earthquake Engineering. Lecture Notes in Civil Engineering, vol 175*, S. Kolathayar and S. C. Chian, Eds., Singapore: Springer, Sep. 2021, pp. 161–174. doi: 10.1007/978-981-16-4617-1_13.

[37] R. Doroudi, S. H. H. Lavassani, M. Shahrouzi, and M. Dadgostar, "Identifying the Dynamic Characteristics of Super Tall Buildings by Multivariate Empirical Mode Decomposition," *Struct Control Health Monit*, Aug. 2022, doi: 10.1002/stc.3075.

[38] SNI 2847:2019, "Persyaratan Beton Struktural untuk Bangunan Gedung dan Penjelasan," 2019.

[39] G. D'Arenzo, P. Rigo, V. Nicolussi, L. Pozza, and D. Casagrande, "Characterisation of the Rigid Diaphragm Conditions for Cross Laminated Timber Floors," *Bulletin of Earthquake Engineering*, vol. 23, pp. 1759–1794, Mar. 2025, doi: 10.1007/s10518-024-02025-5.

[40] D. K, R. Madihalli, L. M. S., N. K. B. M., and R. H. C., "Study on Influence of Rigid and Semi Rigid Diaphragm System on RC Structure," in *2022 International Interdisciplinary Humanitarian Conference for Sustainability (IIHC)*, Bengaluru, India: IEEE, Nov. 2022, pp. 7–11. doi: 10.1109/IIHC55949.2022.10060573.

[41] M. A. Masrom and N. H. A. Hamid, "Finite Element Study: Rocking Wall-Floor Connection of Precast Concrete Load-Bearing Structures Subjected to Quasi-Static Lateral Loading," *Journal of Earthquake Engineering*, vol. 27, no. 7, pp. 1711–1739, Jul. 2022, doi: 10.1080/13632469.2022.2087797.

[42] M. A. Afshar, S. Aghaeipour, M. R. A. Parvar, and A. A. Mazloum, "Optimal Dynamic Performance of Partially Base-Isolated Structure under Seismic Excitations: Harmonic, Earthquake, and Random," *Structures*, vol. 55, pp. 263–277, Sep. 2023, doi: 10.1016/j.istruc.2023.05.110.

[43] J. Zhao, Z. Tan, R. Yu, Z. Li, X. Zhang, and P. Zhu, "Deformation Responses of the Foundation Pit Construction of the Urban Metro Station: A Case Study in Xiamen," *Tunnelling and Underground Space Technology*, vol. 128, no. 104662, Oct. 2022, doi: 10.1016/j.tust.2022.104662.

[44] SNI 1727-2020, "Beban Desain Minimum dan Kriteria Terkait untuk Bangunan," 2020.

[45] F. Nadiar *et al.*, "Comparative Analysis of Deviation in High Buildings Based on Earthquake Load SNI 1726:2012 and SNI 1726:2019," in *E3S Web Conf. Volume 513, 2024*, International Conference on SDGs for Sustainable Future (ICSSF 2024), Jul. 2024, p. 01008.

[46] N. E. Saputra and Y. A. Priastiwi, "Comparative Study of Dynamic Earthquake Analysis with Spectral Design and Time History Methods," *Jurnal Indonesia Sosial Teknologi*, vol. 4, no. 8, pp. 1223–1234, Aug. 2023, doi: https://doi.org/10.59141/jist.v4i8.700.

[47] M. S. Thordal, J. Chr. Bennetsen, and H. H. H. Koss, "Review for Practical Application of CFD for the Determination of Wind Load on High-Rise Buildings," *Journal of Wind Engineering and Industrial Aerodynamics*, vol. 186, pp. 155–168, Mar. 2019, doi: 10.1016/j.jweia.2018.12.019.

[48] E. Gavanski and H. Nishimura, "Wind Loads on Multi-Span Roof Buildings," *Journal of Wind Engineering and Industrial Aerodynamics*, vol. 220, no. 104824, Jan. 2022, doi: 10.1016/j.jweia.2021.104824.

[49] J. Sunaryati, Yulianti, Nidiasari, and V. Anggraini, "Structural Analysis Due to Wind Speed as Static Loads on Building," in *The 2nd International Conference on Disaster Mitigation and Management (2nd ICDMM 2023)*, E3S Web of Conferences 464, 15009 (2023), Dec. 2023. doi: 10.1051/e3sconf/202346415009.

[50] B. Yan, Y. Yuan, C. Ma, Z. Dong, H. Huang, and Z. Wang, "Modeling of Downburst Outflows and Wind Pressures on a High-Rise Building Under Different Terrain Conditions," *Journal of Building Engineering*, vol. 48, no. 103738, May 2022, doi: 10.1016/j.jobe.2021.103738.

[51] G. Fang, M. Wei, L. Zhao, K. Xu, S. Cao, and Y. Ge, "Site-and Building Height-Dependent Design Extreme Wind Speed Vertical Profile of Tropical Cyclone," *Journal of Building Engineering*, vol. 62, no. 105322, Dec. 2022, doi: 10.1016/j.jobe.2022.105322.

[52] S. Saxena and M. Patel, "Evaluating Dynamic Behaviour of a Concrete dam using Modal Analysis," *Mater Today Proc*, vol. 93, no. 3, pp. 296–301, 2023, doi: 10.1016/j.matpr.2023.07.259.

[53] Z. Dong, L. Yan, and H. Su, "Modal Analysis of An External Rotor Machine For Electric Propulsion Aircraft," in *2022 IEEE 17th Conference on Industrial Electronics and Applications (ICIEA)*, Chengdu, China: IEEE, 2022, pp. 1658–1662. doi: 10.1109/ICIEA54703.2022.10006278.

[54] M. Zhao, Z. Gao, P. Wang, and X. Du, "Response Spectrum Method for Seismic Analysis of Monopile Offshore Wind

Turbine," *Soil Dynamics and Earthquake Engineering*, vol. 136, no. 106212, Sep. 2020, doi: 10.1016/j.soildyn.2020.106212.

[55] K. P. S. Sundar, M. K. Shrimali, S. D. Bharti, and A. Vibhute, "Seismic Response Analysis of Concrete Gravity Dam Using Response Spectrum Analysis and Response History Analysis," in *Proceedings of 17th Symposium on Earthquake Engineering (Vol. 2). SEE 2022. Lecture Notes in Civil Engineering, vol 330*, M. Shrikhande, P. Agarwal, and P. C. A. Kumar, Eds., Singapore: Springer, Feb. 2023, pp. 207–217. doi: 10.1007/978-981-99-1604-7_16.

[56] M. Syarif, S. Astika, and A. Viddy, "Study on the Application of Earthquake Resistant Standards (SNI 1726: 2019) Against Building in Yogyakarta City," in *Proceedings of the 5th International Conference on Applied Science and Technology on Engineering Science (iCAST-ES 2022)*, Science and Technology Publications, Lda, 2022, pp. 148–153. doi: 10.5220/0011729600003575.

[57] A. Joshi, A. Pal, and A. Vishwakarma, "Determination of Performance Point of Stability Improvement of the Multistoried Building using Different Grade of Concrete in Beams at Different Levels over Soft Soil: A Review," *International Journal Advanced Engineering Research and Science*, vol. 7, no. 8, Aug. 2020, doi: 10.22161/ijaers.78.25.

[58] M. M. A. Pratama, S. Abifurrizal, Y. Novitasari, W. Damayanthi, P. Puspitasari, and Avita A. Permanasari, "Potential Use of Graded Concrete as Structural Elements of Multi-Storey Buildings," in *Journal of Physics: Conference Series, Volume 1833, International Conference on Technology and Vocational Teachers (ICTVT)*, Yogyakarta, Indonesia: Journal of Physics: Conference Series, Oct. 2021. doi: 10.1088/1742-6596/1833/1/012040.